Check for updates

Fabrication of Graphene Oxide and Nanohydroxyapatite Reinforced Gelatin–Alginate Nanocomposite Scaffold for Bone Tissue Regeneration

Shiv Dutt Purohit[1], Hemant Singh[1], Rakesh Bhaskar[2], Indu Yadav[1], Sakchi Bhushan[1], Mukesh Kumar Gupta[2], Anuj Kumar[3]* and Narayan Chandra Mishra[1]*

[1] Department of Polymer and Process Engineering, Indian Institute of Technology Roorkee, Roorkee, India, [2] Department of Biotechnology and Medical Engineering, National Institute of Technology Rourkela, Rourkela, India, [3] School of Chemical Engineering, Yeungnam University, Gyeongsan, South Korea

Graphene oxide (GO) and nanohydroxyapatite (nHAp) proved to be a potential material for bone tissue-regeneration applications. Therefore, GO and nHAp reinforced porous polymeric nanocomposite scaffolds have been gaining significant research thrust. In this study, GO and nHAp based nanocomposite was synthesized and used as a reinforcing agent to develop gelatin-alginate (GA)-based three-dimensional porous polymeric nanocomposite scaffold. The polymeric nanocomposite scaffold (nHAp-GO/GA) was fabricated by using freeze-drying process, which may show a synergistic effect of each of the components for tissue regeneration. The scaffold demonstrates good physico-chemical properties. The porous microstructure of the scaffold is evidenced by Field emission scanning electron microscopy (FESEM). High swelling of the scaffold in presence water, indicates that the scaffold is highly hydrophilic, which implies the suitability of the scaffold for tissue regeneration. Further, the incorporation of nHAp-GO enhances the compressive strength of the scaffold while reduces the rate of biodegradation, which is good for bone tissue engineering. The scaffold is biocompatible. *In vitro* cell study with MG-63 bone cells demonstrates the synergistic effect of each of the components of the scaffold, on mineral deposition. Therefore, it can be concluded that nHAp-GO/GA polymeric nanocomposite scaffold can be a potential candidate for bone tissue regeneration.

Keywords: graphene oxide, nanohydroxyapatite, bone tissue engineering and regeneration, nanocomposite, gelatin, alginate

INTRODUCTION

Bone is made of inorganic and organic composites. It mainly consists of calcium phosphorus salts and collagen. This amalgamation of inorganic-organic characteristics aid in load bearing capabilities, and it also acts as a reservoir for minerals in the body; which in turn helps in maintaining calcium ions homeostasis (Puska et al., 2011; Sheikh et al., 2015; Winkler et al., 2018).

The bone defects (i.e., bone fractures and cranial-maxillofacial traumatic injuries) have become a major health challenge. Currently, metallic implants or bone grafts are being used for the treatment of bone defects, but shortcomings of the current treatments such as complex surgical procedure, donor-site morbidity, immune rejection, and hindered functional recovery have garnered the research impetus to develop novel biomaterials (Buckwalter et al., 1996; Purohit et al., 2019).

In recent years, a variety of materials (i.e., ceramics, metals, and polymers) have been explored. The disadvantages like complex processability and non-degradability restricts the use of ceramics and metals (Maquet and Jerome, 1997; Liu and Ma, 2004). Therefore, various natural and synthetic polymers, and nanomaterials or their combinations have gained significant research thrust to find the ideal bone substitute (Polo-Corrales et al., 2014; Singh et al., 2014, 2015; Kang et al., 2015; Kumar et al., 2019). Apart from other inorganic materials, nanohydroxyapatite (nHAp) has been acknowledged largely owing to its biocompatibility, slow degradation, osteoconductivity and bone integration ability. However, the brittleness and poor flexibility of nHAp restricts its use in bone regeneration applications on its own (Bundela and Bajpai, 2008; Zhou and Lee, 2011; Salmasi et al., 2016). To overcome these shortcomings of nHAp, it is incorporated with other nanomaterials and/or polymeric scaffolds (Salmasi et al., 2016). In this regard, graphene oxide (GO) and natural polymers (i.e., gelatin, alginate, fibrin, etc.) have gained significant attention (Deepachitra et al., 2015; Kumar et al., 2019; Purohit et al., 2019).

Graphene oxide, a graphene-derivative has distinctive properties such as large surface area, good mechanical and chemical properties (Deepachitra et al., 2015; Kumar et al., 2019; Purohit et al., 2019). Additionally, the functional groups present on the GO surface offer reactive sites, which enable it to facilitate cellular adhesion and chemical interactions with other materials (Deepachitra et al., 2015; Janković et al., 2015; Kumar et al., 2018). These exceptional properties make GO a potential material for its use in biomedical applications. Still, GO could not provide proper three-dimensional microarchitecture, which is essential for large bone defects. Therefore, nanomaterials incorporated polymeric scaffolds found to be suitable due to their easy processability and three-dimensional microarchitecture.

Gelatin, a natural polymer with structural similarity to collagen, is widely used owing to its abundant availability, easy processability into various shapes, biodegradability, biocompatibility and cost effectiveness. In addition, gelatin has RGD (Arg–Gly–Asp) peptide sequences, which facilitates cellular proliferation (Purohit et al., 2019). But, the limitations like low elasticity, poor mechanical strength and shape stability restricts its use in hard tissue engineering applications (Dash et al., 2013; Xing et al., 2014). Therefore, alginate, a polysaccharide consisting of β-d-mannuronate (M-blocks) and α-l-guluronate (G blocks) residues with β (1–4) glycosidic linkage, has been widely used for the fabrication of hydrogel-based scaffolds owing to its easy crosslinking ability with Ca^{2+} ions and adequate mechanical strength (McHugh, 1987; Sharma et al., 2016).

Thus, looking at the vital role of materials in treating orthopedic complications, the authors have fabricated the nanocomposite scaffold of inorganic and organic composite nature. For this purpose nHAp-GO nanocomposite has been synthesized and reinforced to the gelatin-alginate (GA) polymeric blend to obtain the nHAp-GO/GA nanocomposite scaffold. Further, the fabricated scaffolds were characterized by field emission scanning electron microscopy (FESEM), swelling and *in vitro* degradation, mechanical properties and *in vitro* cell culture.

MATERIALS AND METHODS

Materials

Gelatin (from bovine skin), alginic acid, sodium salt and alkaline phosphatase (AP), leukocytes staining kit were purchased from Sigma-Aldrich (MO, United States). Calcium chloride and ammonium hydroxide were purchased from Merck. Glutaraldehyde, *N*-hydroxysuccinimide (NHS), 1-ethyl-3-(3-dimethylaminopropyl)carbodiimide (EDC), EZ Stain osteocyte staining kit, EZ Assay Alkaline phosphatase activity estimation kit, calcium hydroxide, ortho-phosphoric acid, sodium hydroxide, ethanol, phosphate buffer saline (PBS), sodium bicarbonate, fetal bovine serum (FBS), trypsin-EDTA, antibiotic-antimycotic solution, alpha minimum essential medium (α-MEM), and L-ascorbic acid were purchased from HiMedia (India). MilliQ distilled water was used throughout the experiments. GO was synthesized using graphite powder, 100 micron (S-D fine chemicals, India).

Synthesis of nHAp-GO Nanocomposite

nHAp-GO nanocomposite was synthesized by adding 0.1 M $Ca(OH)_2$ into 24 ml of 4% ethanol solution and stirring for 30 min. Thereafter, 0.1 M H_3PO_4 in 3.6 ml distilled water was added slowly to the developed solution. A total of 10 ml GO nanoparticles (see **Supplementary Material** for "Synthesis Method") solution (1.0 mg/1.0 ml) was added to the above solution. The above solution was then stirred vigorously with pH above 10. After 2 h of stirring at 60°C, the solution was aged for 24 h. The precipitate was collected and washed with distilled water. Finally, the precipitate was dried in a vacuum oven at 80°C.

Fabrication of GA and Nanocomposite Scaffolds

For the fabrication of GA scaffold, 10wt% alginate and gelatin were solubilized in distilled water separately. Then equal ratio of both the solution was mixed and stirred for 6 h to obtain GA polymer blend. Further, certain volume of GA solution was casted in various tissue culture plates (TCP) to fabricate scaffolds of preferred diameter and thickness. Thereafter, the TCP were kept in refrigerator for 2 h to induce gelation in the GA polymeric blend. Then the resulting scaffolds were taken out and immersed in 1 M $CaCl_2$ solution for 2 h to chemically crosslink alginate molecules with calcium ions. Next scaffolds were washed thoroughly and kept in the 2wt% EDC and 0.25wt% NHS in 80vol% ethanol solution for 12 h at 4°C to induce crosslinking of gelatin molecules (Liang et al., 2004; Purohit et al., 2019). Lastly,

the scaffolds were thoroughly washed with double distilled water and kept at −20°C for 12 h followed by lyophilization of the obtained scaffolds.

For the fabrication of nHAp-GA, GO-GA and nHAp-GO/GA nanocomposite scaffolds, 2 wt/vol% of nHAp, GO and nHAp-GO suspensions in GA polymeric blend were prepared. Then, these suspensions were stirred vigorously for 6 h followed by ultra-sonication. All the further steps for scaffold fabrication were similar to the steps used for GA scaffold fabrication.

Field Emission Scanning Electron Microscopy (FESEM)

Morphology and topography of the nHAp-GO nanocomposite were analyzed by FESEM (TESCAN Mira 3 Scanning Electron Microscope) (Purohit et al., 2019). In brief, nanoparticles were sputter coated with gold to minimize the charging of the samples. nHAp-GO nanocomposite was imaged at 15–20 kV beam energy. Energy dispersive X-ray spectroscopy (EDS) was performed to evaluate the elemental composition of nHAp-GO. EDS was carried out at beam energy 18 kV on FESEM equipped with EDAX, AMTEK, United States. The detector has a resolution of 126.5 eV at MnKα.

Dynamic Light Scattering and Zeta Potential Analysis

Zeta potential and dynamic light scattering (DLS) analysis of the nHAp-GO nanocomposite were carried out in distilled water using a Zetasizer Nano (Malvern, Worcestershire, United Kingdom) at 25°C in a quartz cuvette. The results obtained for zeta potential and mobility by zeta potential analysis, and mean size (nm) and polydispersity by DLS analysis are depicted as the mean ± standard deviation (SD). All the tests were performed in triplicates (Nanda, 2016).

X-Ray Diffraction Spectroscopy (XRD)

X-ray diffraction spectroscopy of the nHAp-GO nanocomposite was performed by X-ray diffractometer (RigakuUltima IV) using a CuKα radiation source. Scans were performed at 2θ values in the range of 5°–50° at a rate of 4°/min (Purohit et al., 2019).

Porosity

The Porosity of the composite scaffold nHAp-GO/GA was measured by liquid displacement method. In short, the developed scaffold sample was kept in a graduated cylinder filled with the known concentration of ethanol solution (V_a). The raised volume of solution after scaffold immersion was noted as V_b. Further, the scaffold was removed and the volume of ethanol solution left in the cylinder (V_c) was noted. The total volume V_t of the scaffold was calculated using equations shown below:

$$V_t = V_b - V_c \qquad (1)$$

The porosity χ was determined using the Eq 2

$$\chi = \frac{V_a - V_c}{V_t} \qquad (2)$$

Porosity of each sample was tested for five times and the average porosity with SD was calculated (Sharma et al., 2016).

In vitro Degradation

In this study, known weight (W_i) of the developed scaffold samples have been placed in PBS for 28 days (Purohit et al., 2019). To determine the degradation rate, the scaffolds were removed from PBS after every 7 days, thoroughly washed with distilled water, dried, and weighed (W_f). Change in mass or percentage weight loss (%WL) of the developed scaffold samples were calculated as per the following equation:

$$\%WL = \frac{W_i - W_f}{W_i}$$

Swelling

For measuring swelling rate, known dry weight (W_d) of each scaffold was measured first (Sharma et al., 2016). Then, these scaffold samples were placed in PBS at room temperature. At regular time interval, wet scaffold samples were taken out, soaked in tissue paper and weight (W_s) was noted using electronic weighing balance. The experiment was performed until there is no weight change in the scaffold was observed. The Swelling study was performed on all the samples in triplicate and the% swelling was calculated by the following equation

$$\%Swelling = \frac{W_s - W_d}{W_d} \times 100$$

Mechanical Properties

To assess the mechanical properties of the GA and nHAp-GO/GA nanocomposite scaffolds, compression test was carried out with Instron universal testing machine (Norwood, MA, United States). The scaffold samples with 12 mm diameter and 9 mm height were undergone compression test at strain rate of 1 mm/min. Stress–Strain graph was drawn for each scaffold sample. All the compression tests were performed in triplicates (Kumar et al., 2018).

Cell Culture

For performing all the cell culture related study, MG 63 cell line (pre-mature osteoblast osteosarcoma) was obtained by NCCS, Pune. The cells were cultured in α-MEM media added with 10% FBS and antibiotics inside the CO_2 incubator at 37°C, 5% CO_2 supply with humidity.

Cell Seeding

For culturing cells on the scaffold, uniform sized cylindrical scaffold samples (6 mm diameter; ∼2 mm height) of the polymeric nanocomposite were taken. For sterilization, all the scaffolds were treated with 70% ethanol and ultra-violet light for 30 min, followed by PBS washing. Then, the sterilized scaffolds were placed in the 96-well TCP and the complete media was added. Thereafter, T were kept in CO_2 incubator at 37°C and 5% CO_2 supply for 12 h., After that, cells were seeded at the density of 5,000/cm^2 over the scaffolds. Here, TCP acted as positive control and complete media without cells acted as negative control. At every alternate day media was replaced with fresh media.

MTT Assay

For checking the mitochondrial activity of cells within the scaffold and TCP, a colorimetric MTT assay was performed. After a period of 1-day, 4-day, and 7-day cell seeded TCP and scaffolds were taken, washed with PBS solution. Then, yellow MTT dye was added on the scaffolds and TCP was placed inside the CO_2 incubator for approximately 4 h. further, aliquots were taken out using micropipette and the solubilization buffer was added to dissolve the formazan crystals. Then, OD values of each well were measured using spectrophotometer at a wavelength of 595 nm (Sharma et al., 2016; Kulanthaivel et al., 2017).

Environmental Scanning Electron Microscope (ESEM)

For ESEM characterization, scaffolds seeded with cells were washed with PBS and fixed using gluteraldehyde. Then, scaffolds were dehydrated with different concentrations of ethanol (50, 70, 90, 95, and 100%) for 5 min each. At last, air-dried cell scaffolds were observed under ESEM (Quanta 250 FEG, Thermo Fisher Scientific) (Purohit et al., 2019).

Optical Imaging of MG 63 Cells Over Scaffolds

In this study, TCP, GA, nHAp-GA, GO-GA, and nHAp-GO/GA scaffolds were seeded with MG 63 cells and the cells were cultured for a period of 7 days, after that media was removed and samples were washed with PBS. Further, on the TCP and scaffolds, cells were fixed using methanol and morphology of the cells were observed under inverted microscope.

Osteocyte Staining

EZstain[TM] osteocyte staining kit contains a complete ready to use collection of reagents required for osteocyte staining with alizarin red S. Mineralization on the scaffold surface was measured by quantification of alizarin red staining (ARS). Briefly, cells were fixed in 10% formaldehyde, incubated with 40 mM alizarin red at pH 4.1, washed and air-dried. Then the cell–scaffold constructs were observed under inverted microscope. Thereafter, cell–scaffold constructs were de-stained with 5% perchloric acid and the ARS stain containing perchloric acid solution was transferred to another TCP. Further, the OD values were recorded at 405 nm using microplate reader. Staining was done after day 7 and day 14 of cell seeding. Here, relative matrix deposition is corresponding to the OD values obtained for each scaffold sample.

Alkaline Phosphatase Activity

For alkaline phosphatase (ALP) activity of MG 63 cell line ALP assay kit (Himedia, India) was used. Briefly, the lysates were extracted by digestion of MG 63 cells and reacted with p-nitrophenyl phosphate (p-NPP), Further absorbance of p-nitrophenol was evaluated at 405 nm at the 90 sec time interval for 45 min, by using a microplate reader (Multiscan[TM], Thermo Scientific) to indicate the ALP quantity as nmol of p-nitrophenol per minute. Further, the ALP activity results were normalized with the total DNA content per lysate. For cell ALP staining, AP, leukocyte (sigma Aldrich, United States) was used. Briefly, MG 63 cells, cultured on scaffolds, were fixed with formaldehyde.

Then cell–scaffold constructs were washed with PBS, followed by incubation with FRV-alkaline solution for 30 min. Afterward, stained cell–scaffold constructs were washed with PBS to remove excess stain and the images were captured using phase contrast inverted microscope.

Statistical Analysis

All the experiments were performed in triplicate and experimental results were analyzed by Graph Pad Prism 7 using one way, two way ANOVA and t-test. The results are expressed as mean and SD. The probability $p < 0.05$ was considered to be a statistical difference.

RESULTS AND DISCUSSION

Physicochemical Characterization of nHAp-GO Nanocomposite

In this study, nHAp-GO nanocomposite was synthesized by co-precipitation method and characterized for its morphology and size by FESEM and DLS. In **Figure 1A**, FESEM image obtained for nHAp-GO nanocomposite depicts agglomerated and roughly spherical shaped morphology; similar results were obtained by various researchers for nHAp-GO (Ramani and Sastry, 2014; Deepachitra et al., 2015; Heshmatpour and Haghbin, 2020). The particle size analysis, by DLS analysis (**Figures 1C,E**), shows mean diameter of the synthesized nanocomposite to be 459 ± 51.56 nm and polydispersity 0.307 ± 0.22. This increased size distribution could be explained as mentioned by Nanda (2016) that DLS cannot distinguish among organic and inorganic materials and it calculates the hydrodynamic diameter of the aggregated nanoparticles (Nethi et al., 2017). The elemental composition analysis, in **Figure 1B** by EDS, illustrates the presence of carbon along with oxygen, calcium, and phosphorus. The Ca/P molar ratio was found to be 1.96 which is around the Ca/P ratio 1.67 of nHAp (**Supplementary Figure S2**), the obtained data is consistent with the previous study of biological apatite (Bailey et al., 2009; Deepachitra et al., 2015). Further, zeta potential (**Figure 1C**), which is a critical factor for the nanocomposite stability in a suspension, is found to be -06.47 ± 2.11 mV. The higher surface charge produces the repulsive force between the nanocomposites and hinders the agglomeration. Thus it could be stated that synthesized nanocomposites are stable (Nanda, 2016; Nethi et al., 2017). Further, as explained by Abburi and Abburi (2019) surface charge of hydroxyapatite affects cell–membrane interactions. Positively charged nanoparticles can penetrate into cell membranes while negatively charged nanoparticles do not enter the cell at all (Abburi and Abburi, 2019) and the surface charge of the synthesized nHAp-GO is negative, thus it could not enter the cell and it may aid in the surface properties of the resulting scaffold.

Further, to confirm the synthesis of nHAp-GO nanocomposite, XRD analysis was performed on the powder sample. Here, **Figure 1D** demonstrates the XRD spectra for the GO, nHAp and nHAp-GO nanocomposite. Here, nHAp-GO depicts the distinctive x-ray diffraction peaks at 25.86°, 31.7°, and 32.83° corresponding to (002), (300), and (202) reflection of nHAp. Further, the characteristic (002) peak of GO at
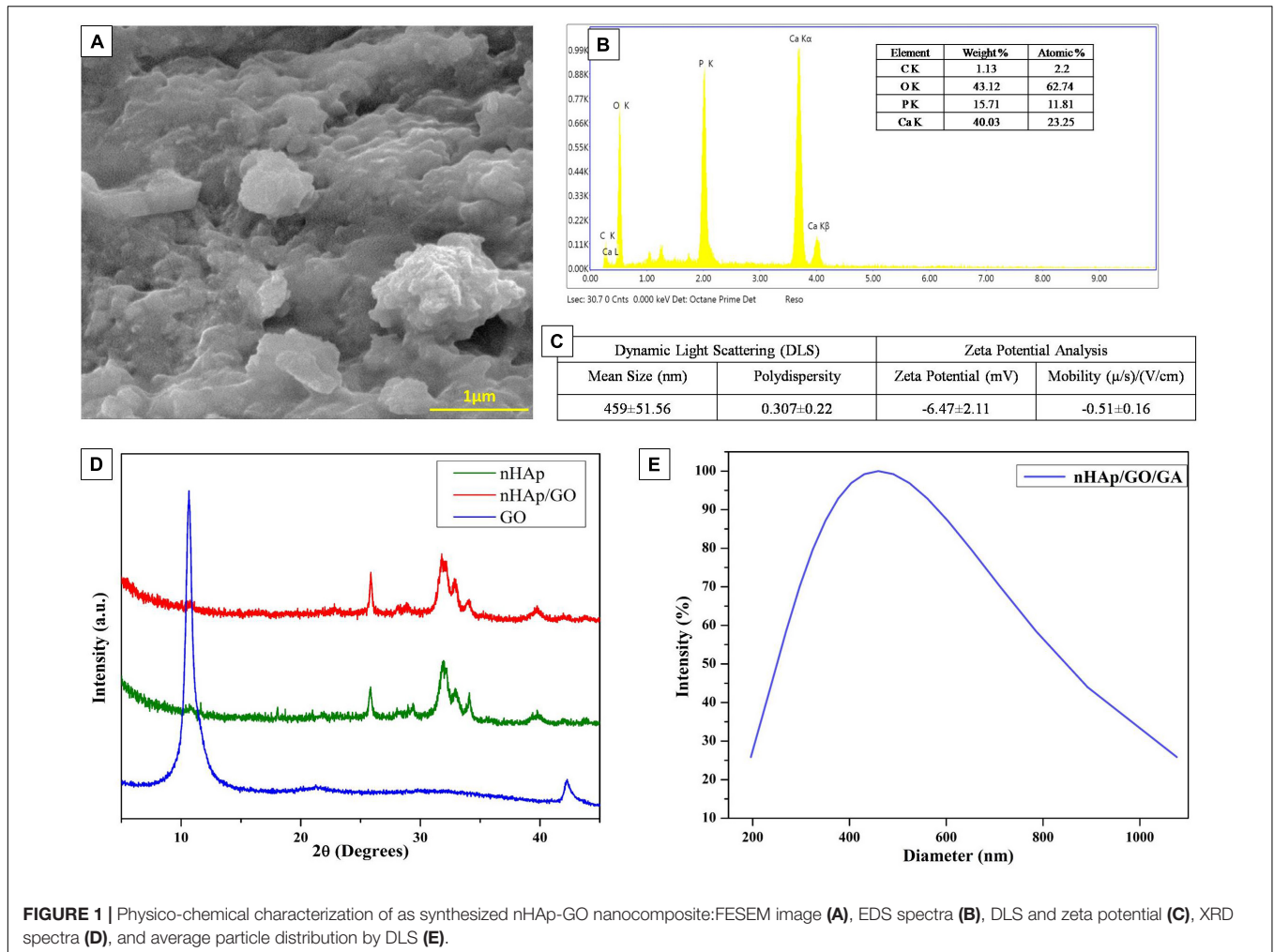
FIGURE 1 | Physico-chemical characterization of as synthesized nHAp-GO nanocomposite:FESEM image **(A)**, EDS spectra **(B)**, DLS and zeta potential **(C)**, XRD spectra **(D)**, and average particle distribution by DLS **(E)**.

10.8° diminished/disappeared. This indicates the successful exfoliation of the GO platelets and the intercalation of the nHAp, similar results were observed by various other researchers (Granados-Correa et al., 2010; Lee et al., 2013; Kumar et al., 2014). Further, FESEM images of GO and nHAp are provided in **Supplementary Figure S1**.

Physical Characterization of nHAp-GO/GA Nanocomposite Scaffold

Figures 2A–D illustrate the microarchitecture of the GA, nHAp-GA, GO-GA, and nHAp-GO/GA scaffolds. The FESEM micrograph depicts the highly porous nature of the scaffolds, and pore-size analysis by ImageJ revealed that the pore diameter of the scaffolds is in the range of 70.23–334 μm. Furthermore, the results for the average porosity of the scaffolds mentioned in **Figure 2E** indicate porosity values for GA scaffold is ∼86% and for nHAp-GO/GA scaffold porosity is about 79%. The difference in the porosity could be due to the deposition of the nHAp-GO nanocomposite. The results obtained for porosity comply with reported works of literature (Sharma et al., 2016; Purohit et al., 2019).

The obtained results for pore size and porosity are key to the scaffold properties because the pores assist in cellular proliferation and migration, in addition to support vascularization during neo tissue formation. Earlier reported studies suggest that the minimum required pore size for bone tissue regeneration is around 100 μm. Still, pore sizes between 200 and 300 μm are considered to be most suitable for adequately mineralized bone formation and vascularization, which aids in the osteogenesis (Serafim et al., 2015). Furthermore, the porosity, in the range from 50 to 90% is considered to be optimum as it assists in achieving the desired physical and biological properties of the scaffolds (Mishra et al., 2019). From *in vitro* biodegradation pattern (**Figure 2F**), it is evident that after 28 days of degradation studies, degradation percentage for GA, nHAp-GA, GO-GA, and nHAp-GO/GA scaffolds are 53.8, 46.0, 30.45, and 29.4, respectively. This decrease in degradation percentage for nHAp-GO/GA scaffold could be attributed to an increase in the physical cross-linkage between the GA and nHAp-GO. Similar results for nHAp and nHAp-GO with other scaffolds were reported in the literature (Ramani and Sastry, 2014; Deepachitra et al., 2015). The slow degradation achieved by the nHAp-GO/GA scaffold is advantageous for bone tissue engineering.
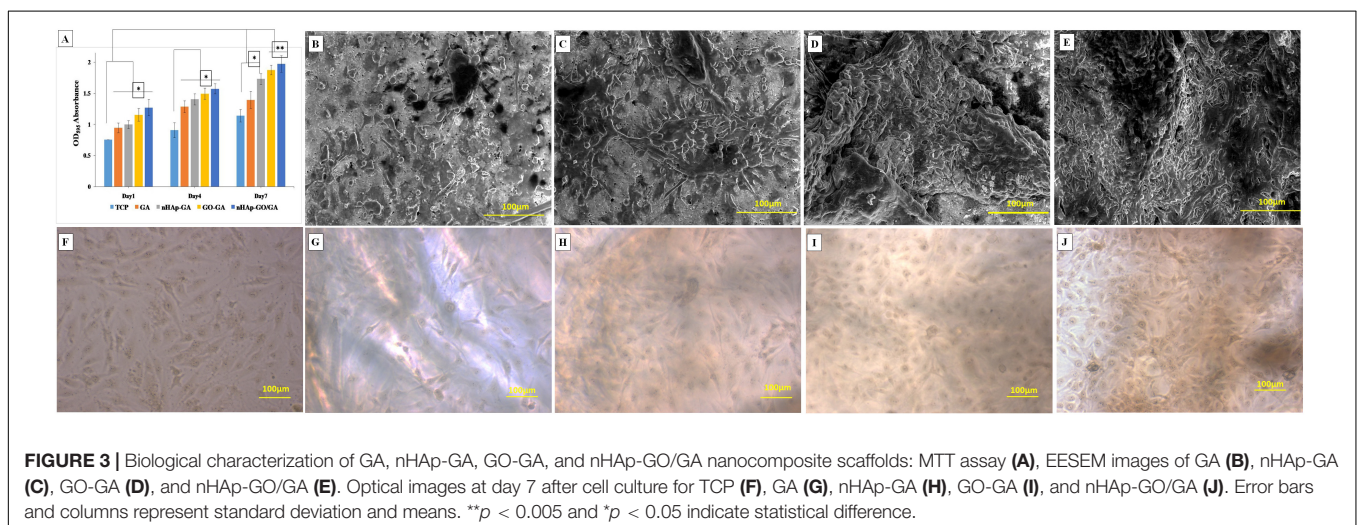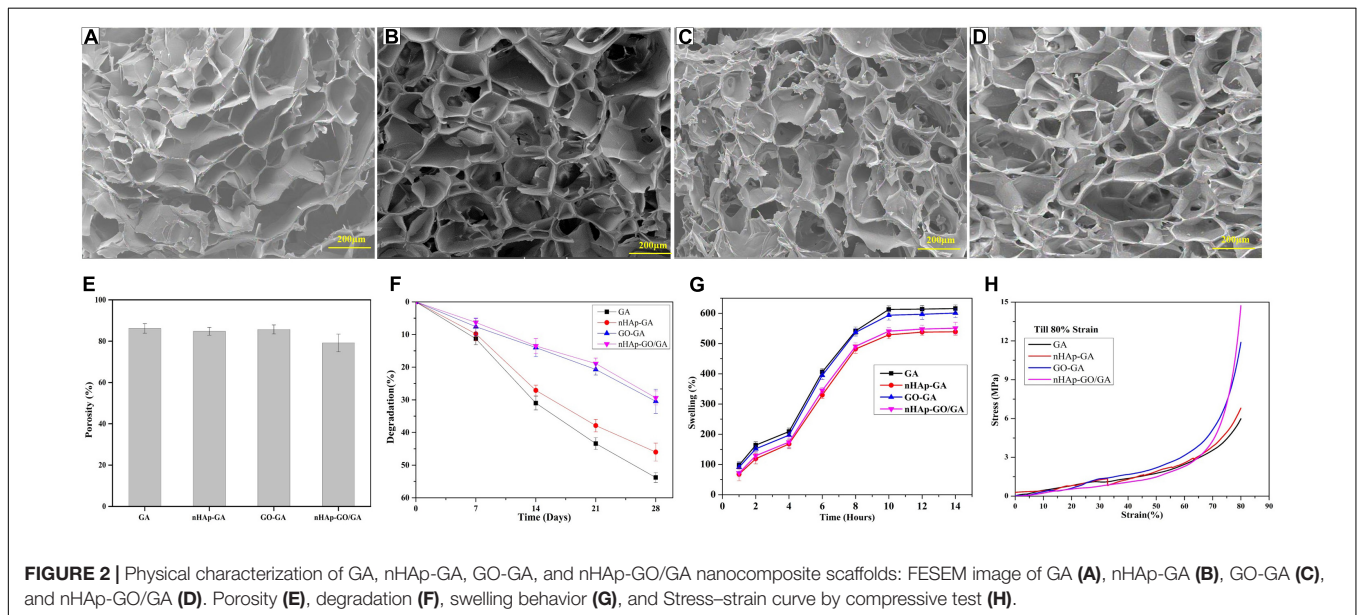
Figure 2G exhibits %swelling of GA, nHAp-GA, GO-GA, and nHAp-GO/GA scaffolds: all the scaffolds are hydrophilic in nature. Here, the GA scaffold has the highest %swelling at 629% and the lowest %swelling at 539% is observed in the nHAp-GA scaffold, while GO-GA and nHAp-GO/GA showed 601 and 551% swelling respectively. The results indicate that addition of GO aid in hydrophilicity of the nanocomposite scaffolds. For all the scaffolds, the %swelling rapidly increased between 1 and 10 h and no significant change occurred after 10 h. This hydrophilic nature of the fabricated scaffolds is vital for bone tissue engineering. As prior reported works of literature imply that the hydrophilic nature of scaffold helps in cell attachment and proliferation (Ali et al., 2019; Purohit et al., 2019).
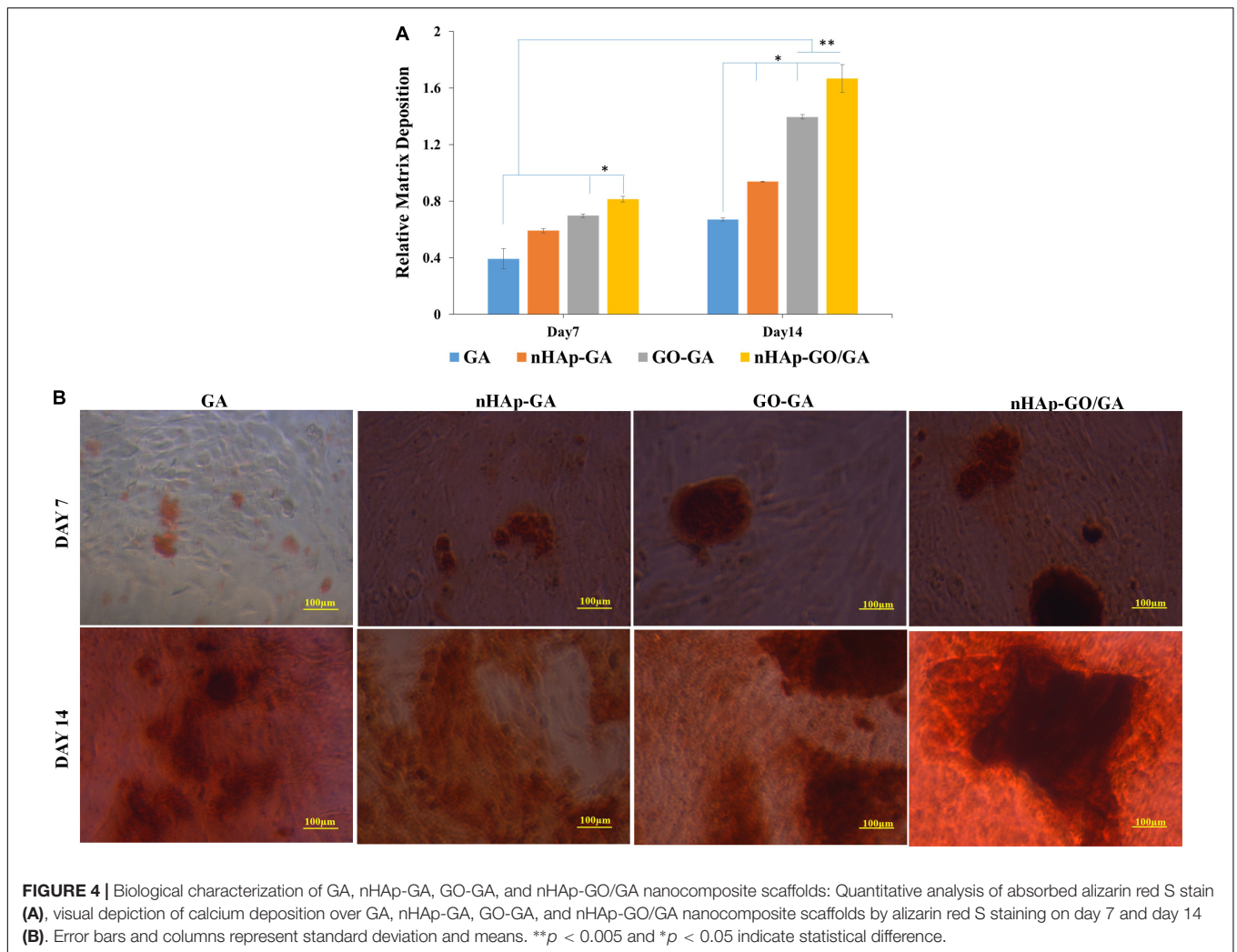
Figure 2H depicts the stress–strain curve at 80% compressive strain, respectively. The mechanical strength, an essential factor for fabricating scaffolds for bone tissue engineering, demonstrates the load bearing capacity of the materials (Gupta et al., 2019). The compressive strength values at 80% strain for GA, nHAp-GA, GO-GA, and nHAp-GO/GA are 5.98, 6.80, 11.89, and 14.72 MPa, respectively. The increase in the compressive strength with the incorporation of nHAp-GO might be attributed to the increase in inter-molecular physical/chemical cross-linking of nHAp-GO with GA. Similar results were observed for the various scaffolds with nHAp and/or GO (Ali et al., 2019; Purohit et al., 2019).

Biological Characterization of nHAp-GO/GA Nanocomposite Scaffold

The MTT assay results (**Figure 3A**) of the scaffolds, revealed a rise in mitochondrial activity as compared to TCP. Moreover, scaffolds containing nHAp-GO nanocomposite showed a significant increase in mitochondrial activity when compared

FIGURE 2 | Physical characterization of GA, nHAp-GA, GO-GA, and nHAp-GO/GA nanocomposite scaffolds: FESEM image of GA **(A)**, nHAp-GA **(B)**, GO-GA **(C)**, and nHAp-GO/GA **(D)**. Porosity **(E)**, degradation **(F)**, swelling behavior **(G)**, and Stress–strain curve by compressive test **(H)**.

FIGURE 3 | Biological characterization of GA, nHAp-GA, GO-GA, and nHAp-GO/GA nanocomposite scaffolds: MTT assay **(A)**, EESEM images of GA **(B)**, nHAp-GA **(C)**, GO-GA **(D)**, and nHAp-GO/GA **(E)**. Optical images at day 7 after cell culture for TCP **(F)**, GA **(G)**, nHAp-GA **(H)**, GO-GA **(I)**, and nHAp-GO/GA **(J)**. Error bars and columns represent standard deviation and means. **$p < 0.005$ and *$p < 0.05$ indicate statistical difference.

FIGURE 4 | Biological characterization of GA, nHAp-GA, GO-GA, and nHAp-GO/GA nanocomposite scaffolds: Quantitative analysis of absorbed alizarin red S stain **(A)**, visual depiction of calcium deposition over GA, nHAp-GA, GO-GA, and nHAp-GO/GA nanocomposite scaffolds by alizarin red S staining on day 7 and day 14 **(B)**. Error bars and columns represent standard deviation and means. **$p < 0.005$ and *$p < 0.05$ indicate statistical difference.
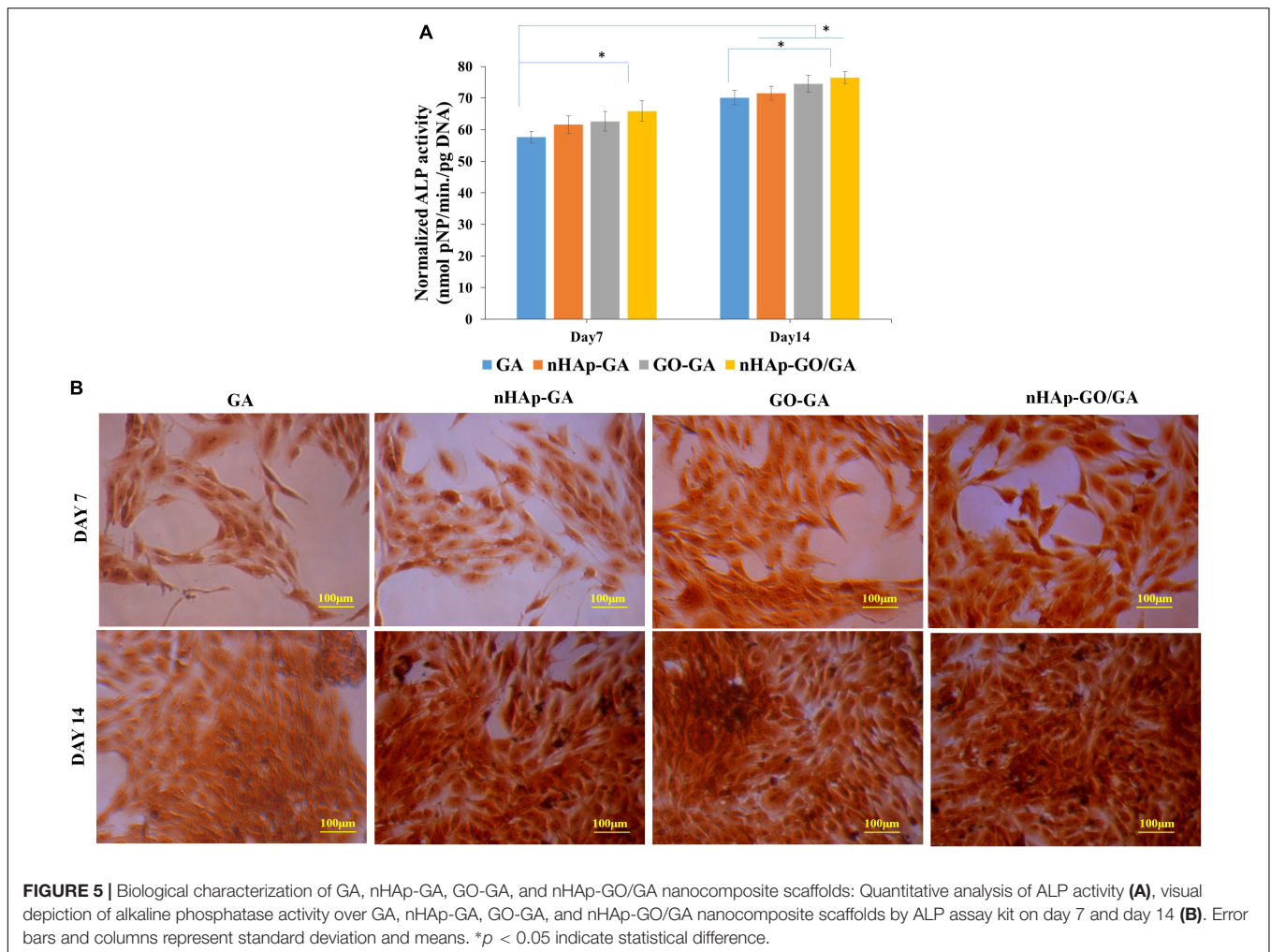
to TCP and GA scaffold. The OD_{595} values corresponding to mitochondrial activity for nHAp-GO/GA nanocomposite scaffold at day 7 is 1.973 as compared to 1.141, 1.391, 1.731, and 1.874 of TCP, GA, nHAp-GA, and GO-GA scaffolds respectively. It could be observed that all the scaffolds showed higher OD_{595} values than TCP. Hence, all the scaffolds are non-cytotoxic and biocompatible. The increased mitochondrial activity could be due to the beneficial effects of the apatite, GO and topography of the nanocomposite scaffold (i.e., an abundance of reactive sites and hydrophilic nature) (Buckwalter et al., 1996; Wan et al., 2014; Purohit et al., 2019).

Further, the morphology of cells at day 7, cultured on TCP, GA, nHAp-GA, GO-GA, and nHAp-GO/GA nanocomposite scaffold, was observed under the optical microscope after cell fixation by methanol, as shown in **Figures 3F–J**. Large cells with polygonal and spindle-shaped morphology along with prominent spherical nuclei are observed which exhibits morphological features specific to MG 63 cell line. Similar kind of healthy and viable cells were also observed proliferating efficiently by various researchers for GA based scaffold or scaffolds with nHAp (Gautam et al., 2013; Gupta et al., 2013; Wang et al., 2016).

ESEM analysis for GA, nHAp-GA, GO-GA, and nHAp-GO/GA nanocomposite scaffold depicts competent cell adhesion to the scaffold surface. The cell morphology observed is in accordance with that observed by optical microscopy. **Figures 3B–E** showed the ESEM images of MG 63 cells grown on scaffolds after 7 days of cell culture, cells were found to attach and spread well on scaffolds. Besides, MG 63 cells spread, migrated and proliferated to confluence over the nHAp-GO/GA scaffold. The results of the morphological analysis are in correlation with the results of MTT assay and previously reported literature (Ramani and Sastry, 2014; Deepachitra et al., 2015). The increase in the cell attachment and cell viability could be attributed to the abundant reactive sites present in the nHAp and GO (Ramani and Sastry, 2014; Deepachitra et al., 2015; Heshmatpour and Haghbin, 2020). This further establishes that a nanocomposite scaffold is a potential candidate for bone regeneration applications.

Further, the alizarin red S staining results are depicted in **Figure 4**. **Figure 4B** demonstrates the visual depiction of the calcium deposition on day 7 and day 14 by MG 63 cells over the GA, nHAp-GA, GO-GA, and nHAp-GO/GA

FIGURE 5 | Biological characterization of GA, nHAp-GA, GO-GA, and nHAp-GO/GA nanocomposite scaffolds: Quantitative analysis of ALP activity **(A)**, visual depiction of alkaline phosphatase activity over GA, nHAp-GA, GO-GA, and nHAp-GO/GA nanocomposite scaffolds by ALP assay kit on day 7 and day 14 **(B)**. Error bars and columns represent standard deviation and means. $*p < 0.05$ indicate statistical difference.

nanocomposite scaffold. Here, it could be observed that nHAp-GO/GA nanocomposite scaffold showed more calcium deposition as compared to other scaffolds. Besides, quantitative alizarin red S staining results (**Figure 4A**), are also consistent with the staining images. Thus it could be stated that induction of nHAp-GO nanocomposite to GA has increased the mineral deposition in the scaffold matrix, in turn promoting the neo bone formation and the other researchers have also observed the similar results for the alginate based scaffolds (Zhou and Xu, 2011; Kulanthaivel et al., 2017). ALP assay was also carried out to confirm the ALP activity, which is a characteristic feature of osteoblast phenotype. The results of the ALP assay are shown in **Figure 5**. It can be observed that the ALP activity for nHAp-GO/GA nanocomposite scaffold is statistically higher than that of GA scaffold (**Figure 5A**). The quantitative results are consistent with the visual images shown in **Figure 5B**. Overall, the ALP activity for the nanocomposite scaffold increased and the normalized ALP activity value on day 14 for nHAp-GO/GA nanocomposite scaffolds was found to be 1.09 fold higher than those obtained for GA. Earlier, it was also reported that addition of the bioactive nanomaterials, i.e., nHAp-GO, caused an increase in the ALP activity

and matrix deposition by MG-63 cells (Ramani and Sastry, 2014; Deepachitra et al., 2015). This increase in ALP activity implies active bone formation which confirms that fabricated nanocomposite scaffolds could be a potential osteoinductive materials for bone regeneration applications (Kulanthaivel et al., 2017; Purohit et al., 2019).

CONCLUSION

In this study, nHAp-GO nanocomposite was synthesized and a novel nHAp-GO reinforced GA (nHAp-GO/GA) nanocomposite scaffold was fabricated by using solvent casting and freeze drying method. The amalgamation of nHAp-GO and GA depicted the synergistic effect on the properties of nanocomposite scaffold. The nHAp-GO nanocomposite provided a large number of functional group (i.e., hydroxy, epoxy, and carboxylic), which enhanced the electrostatic interaction and hydrogen bonding during the nHAp-GO/GA nanocomposite scaffold fabrication. The physical and biological properties of the GA, nHAp-GA, GO-GA, and nHAp-GO/GA nanocomposite scaffold were systemically evaluated via various

analysis techniques, i.e., swelling, degradation, mechanical, and *in vitro* studies. The %swelling and *in vitro* degradation for nHAp-GO/GA nanocomposite scaffold have decreased, while mechanical properties (under compression) have increased drastically. Further, the MG-63 cells cultured over the nHAp-GO/GA nanocomposite scaffold, depicts all the scaffolds are biocompatible. Enhanced calcium deposition and ALP activity were also observed. Based on the findings, it could be stated that the nHAp-GO/GA nanocomposite scaffold may have a potential for the applicability in the bone tissue regeneration.

DATA AVAILABILITY STATEMENT

All datasets generated for this study are included in the article/**Supplementary Material**.

AUTHOR CONTRIBUTIONS

FUNDING

ACKNOWLEDGMENTS

SUPPLEMENTARY MATERIAL

The Supplementary Material for this article can be found online at: https://www.frontiersin.org/articles/10.3389/fmats.2020.00250/full#supplementary-material

REFERENCES

Abburi, A., and Abburi, V. R. (2019). "Controlled synthesis of hydroxyapatite nanoparticles," in *Proceedings of the 2019 IEEE 14th International Conference on Nano/Micro Engineered and Molecular Systems (NEMS)* (Bangkok: IEEE), 300–303.

Ali, A., Bano, S., Priyadarshi, R., and Negi, Y. S. (2019). Effect of carbon based fillers on properties of Chitosan/PVA/βTCP based composite scaffold for bone tissue engineering. *Mater. Today Proc.* 15, 173–182. doi: 10.1016/j.matpr.2019.04.189

Bailey, M. J., Coe, S., Grant, D. M., Grime, G. W., and Jeynes, C. (2009). Accurate determination of the Ca: P ratio in rough hydroxyapatite samples by SEM-EDS, PIXE and RBS—a comparative study. *X Ray Spectr.* 38, 343–347. doi: 10.1002/xrs.1171

Buckwalter, J. A., Glimcher, M. J., Cooper, R. R., and Recker, R. (1996). Bone biology. I: Structure, blood supply, cells, matrix, and mineralization. *Instr. Course Lect.* 45, 371.

Bundela, H., and Bajpai, A. K. (2008). Designing of hydroxyapatite-gelatin based porous matrix as bone substitute: correlation with biocompatibility aspects. *Express Polym. Lett.* 2, 201–213. doi: 10.3144/expresspolymlett.2008.25

Dash, R., Foston, M., and Ragauskas, A. J. (2013). Improving the mechanical and thermal properties of gelatin hydrogels cross-linked by cellulose nanowhiskers. *Carbohydr. Polym.* 91, 638–645. doi: 10.1016/j.carbpol.2012.08.080

Deepachitra, R., Nigam, R., Purohit, S. D., Kumar, B. S., Hemalatha, T., and Sastry, T. P. (2015). In vitro study of hydroxyapatite coatings on fibrin functionalized/pristine graphene oxide for bone grafting. *Mater. Manufact. Process.* 30, 804–811. doi: 10.1080/10426914.2014.994758

Gautam, S., Dinda, A. K., and Mishra, N. C. (2013). Fabrication and characterization of PCL/gelatin composite nanofibrous scaffold for tissue engineering applications by electrospinning method. *Mater. Sci. Eng. C* 33, 1228–1235. doi: 10.1016/j.msec.2012.12.015

Granados-Correa, F., Bonifacio-Martinez, J., and Serrano-Gomez, J. (2010). Synthesis and characterization of calcium phosphate and its relation to Cr (VI) adsorption properties. *Revista Int. Contaminac. Ambient.* 26, 129–134.

Gupta, P., Agrawal, A., Murali, K., Varshney, R., Beniwal, S., Manhas, S., et al. (2019). Differential neural cell adhesion and neurite outgrowth on carbon nanotube and graphene reinforced polymeric scaffolds. *Mater. Sci. Eng. C* 97, 539–551. doi: 10.1016/j.msec.2018.12.065

Gupta, S. K., Dinda, A. K., Potdar, P. D., and Mishra, N. C. (2013). Modification of decellularized goat-lung scaffold with chitosan/nanohydroxyapatite composite for bone tissue engineering applications. *BioMed Res. Int.* 2013:651945.

Heshmatpour, F., and Haghbin, S. (2020). Nanohydroxyapatite/graphene oxide nanocomposites modified with synthetic polymers: promising materials for bone tissue engineering applications. *Int. J. Polym. Mater. Polym. Biomater.* 1–7. doi: 10.1080/00914037.2020.1740990

Janković, A., Eraković, S., Mitrić, M., Matić, I. Z., Juranić, Z. D., Tsui, G. C., et al. (2015). Bioactive hydroxyapatite/graphene composite coating and its corrosion stability in simulated body fluid. *J. Alloys Compd.* 624, 148–157. doi: 10.1016/j.jallcom.2014.11.078

Kang, M. S., Kim, J. H., Singh, R. K., Jang, J. H., and Kim, H. W. (2015). Therapeutic-designed electrospun bone scaffolds: mesoporous bioactive nanocarriers in hollow fiber composites to sequentially deliver dual growth factors. *Acta Biomater.* 16, 103–116. doi: 10.1016/j.actbio.2014.12.028

Kulanthaivel, S., Sharan Rathnam, V. S., Agarwal, T., Pradhan, S., Pal, K., Giri, S., et al. (2017). Gum tragacanth–alginate beads as proangiogenic–osteogenic cell encapsulation systems for bone tissue engineering. *J. Mater. Chem. B* 5, 4177–4189. doi: 10.1039/c7tb00390k

Kumar, A., Negi, Y. S., Choudhary, V., and Bhardwaj, N. K. (2014). Microstructural and mechanical properties of porous biocomposite scaffolds based on polyvinyl alcohol, nano-hydroxyapatite and cellulose nanocrystals. *Cellulose* 21, 3409–3426. doi: 10.1007/s10570-014-0339-7

Kumar, A., Rao, K. M., and Han, S. S. (2018). Mechanically viscoelastic nanoreinforced hybrid hydrogels composed of polyacrylamide, sodium carboxymethylcellulose, graphene oxide, and cellulose nanocrystals. *Carbohydr. Polym.* 193, 228–238. doi: 10.1016/j.carbpol.2018.04.004

Kumar, A., Zo, S. M., Kim, J. H., Kim, S. C., and Han, S. S. (2019). Enhanced physical, mechanical, and cytocompatibility behavior of polyelectrolyte complex hydrogels by reinforcing halloysite nanotubes and graphene oxide. *Comp. Sci. Technol.* 175, 35–45. doi: 10.1016/j.compscitech.2019.03.008

Lee, D. S., Pai, Y., and Chang, S. (2013). Effect of thermal treatment of the hydroxyapatite powders on the micropore and microstructure of porous biphasic calcium phosphate composite granules. *J. Biomater. Nanobiotechnol.* 4:114. doi: 10.4236/jbnb.2013.42015

Liang, H. C., Chang, W. H., Liang, H. F., Lee, M. H., and Sung, H. W. (2004). Crosslinking structures of gelatin hydrogels crosslinked with genipin or a water-soluble carbodiimide. *J. Appl. Polym. Sci.* 91, 4017–4026. doi: 10.1002/app.13563

Liu, X., and Ma, P. X. (2004). Polymeric scaffolds for bone tissue engineering. *Ann. Biomed. Eng.* 32, 477–486. doi: 10.1023/b:abme.0000017544. 36001.8e

Maquet, V., and Jerome, R. (1997). Design of macroporous biodegradable polymer scaffolds for cell transplantation. *Mater. Sci. Forum* 250, 15–42. doi: 10.4028/www.scientific.net/msf.250.15

McHugh, D. J. (1987). Production, properties and uses of alginates. Production and Utilization of Products from Commercial Seaweeds. *FAO. Fish. Tech. Pap.* 288, 58–115.

Mishra, R., Varshney, R., Das, N., Sircar, D., and Roy, P. (2019). Synthesis and characterization of gelatin-PVP polymer composite scaffold for potential application in bone tissue engineering. *Eur. Polym. J.* 119, 155–168. doi: 10.1016/j.eurpolymj.2019.07.007

Nanda, H. S. (2016). Surface modification of promising cerium oxide nanoparticles for nanomedicine applications. *RSC Adv.* 6, 111889–111894. doi: 10.1039/c6ra23046f

Nethi, S. K., Nanda, H. S., Steele, T. W., and Patra, C. R. (2017). Functionalized nanoceria exhibit improved angiogenic properties. *J. Mater. Chem. B* 5, 9371–9383. doi: 10.1039/c7tb01957b

Polo-Corrales, L., Latorre-Esteves, M., and Ramirez-Vick, J. E. (2014). Scaffold design for bone regeneration. *J. Nanosci. Nanotechnol.* 14, 15–56.

Purohit, S. D., Bhaskar, R., Singh, H., Yadav, I., Gupta, M. K., and Mishra, N. C. (2019). Development of a nanocomposite scaffold of gelatin–alginate–graphene oxide for bone tissue engineering. *Int. J. Biol. Macromol.* 133, 592–602. doi: 10.1016/j.ijbiomac.2019.04.113

Puska, M., Aho, A. J., and Vallittu, P. (2011). "Polymer composites for bone reconstruction," in *Advances in Composite Materials-Analysis of Natural and Man-Made Materials*, ed. P. Tesinova (London: IntechOpen), 55–68.

Ramani, D., and Sastry, T. P. (2014). Bacterial cellulose-reinforced hydroxyapatite functionalized graphene oxide: a potential osteoinductive composite. *Cellulose* 21, 3585–3595. doi: 10.1007/s10570-014-0313-4

Salmasi, S., Nayyer, L., Seifalian, A. M., and Blunn, G. W. (2016). Suppl-3, M8: nanohydroxyapatite effect on the degradation, osteoconduction and mechanical properties of polymeric bone tissue engineered scaffolds. *Open Orthopaed. J.* 10:900. doi: 10.2174/1874325001610010900

Serafim, A., Petre, D. G., Moraru, L., Cioflan, H. E., Vasile, E., Mastalier-Manolescu, B., et al. (2015). Gelatin-PVP hydrogels with potential skin grafts applications. *Key Eng. Mater.* 638, 38–46. doi: 10.4028/www.scientific.net/kem.638.38

Sharma, C., Dinda, A. K., Potdar, P. D., Chou, C. F., and Mishra, N. C. (2016). Fabrication and characterization of novel nano-biocomposite scaffold of chitosan–gelatin–alginate–hydroxyapatite for bone tissue engineering. *Mater. Sci. Eng. C* 64, 416–427. doi: 10.1016/j.msec.2016.03.060

Sheikh, Z., Najeeb, S., Khurshid, Z., Verma, V., Rashid, H., and Glogauer, M. (2015). Biodegradable materials for bone repair and tissue engineering applications. *Materials* 8, 5744–5794. doi: 10.3390/ma8095273

Singh, R. K., Jin, G. Z., Mahapatra, C., Patel, K. D., Chrzanowski, W., and Kim, H. W. (2015). Mesoporous silica-layered biopolymer hybrid nanofibrous scaffold: a novel nanobiomatrix platform for therapeutics delivery and bone regeneration. *ACS Appl. Mater. Interfaces* 7, 8088–8098. doi: 10.1021/acsami.5b00692

Singh, R. K., Patel, K. D., Lee, J. H., Lee, E. J., Kim, J. H., Kim, T. H., et al. (2014). Potential of magnetic nanofiber scaffolds with mechanical and biological properties applicable for bone regeneration. *PLoS One* 9:e91584. doi: 10.1371/journal.pone.0091584

Wan, Y., Chen, X., Xiong, G., Guo, R., and Luo, H. (2014). Synthesis and characterization of three-dimensional porous graphene oxide/sodium alginate scaffolds with enhanced mechanical properties. *Mater. Express* 4, 429–434. doi: 10.1166/mex.2014.1188

Wang, K., Nune, K. C., and Misra, R. D. K. (2016). The functional response of alginate-gelatin-nanocrystalline cellulose injectable hydrogels toward delivery of cells and bioactive molecules. *Acta Biomater.* 36, 143–151. doi: 10.1016/j.actbio.2016.03.016

Winkler, T., Sass, F. A., Duda, G. N., and Schmidt-Bleek, K. (2018). A review of biomaterials in bone defect healing, remaining shortcomings and future opportunities for bone tissue engineering: the unsolved challenge. *Bone Joint Res.* 7, 232–243. doi: 10.1302/2046-3758.73.bjr-2017-0270.r1

Xing, Q., Yates, K., Vogt, C., Qian, Z., Frost, M. C., and Zhao, F. (2014). Increasing mechanical strength of gelatin hydrogels by divalent metal ion removal. *Sci. Rep.* 4:4706.

Zhou, H., and Lee, J. (2011). Nanoscale hydroxyapatite particles for bone tissue engineering. *Acta Biomater.* 7, 2769–2781. doi: 10.1016/j.actbio.2011.03.019

Zhou, H., and Xu, H. H. (2011). The fast release of stem cells from alginate-fibrin microbeads in injectable scaffolds for bone tissue engineering. *Biomaterials* 32, 7503–7513. doi: 10.1016/j.biomaterials.2011.06.045